Jahn-Teller distortion and magnetic structures in $LaMnO_3$

H. Sawada
Joint Research Center for Atom Technology, Angstrom Technology Partnership, 1-1-4 Higashi, Tsukuba, Ibaraki 305, Japan

Y. Morikawa and K. Terakura
Joint Research Center for Atom Technology, National Institute for Advanced Interdisciplinary Research, 1-1-4 Higashi, Tsukuba, Ibaraki 305, Japan

N. Hamada
Department of Physics, Science University of Tokyo, 2641 Yamazaki, Noda, Chiba 278, Japan
(Received 27 March 1997)

Structural optimization is performed for $LaMnO_3$ with the first-principles pseudopotential method based on the local density approximation (LDA), the generalized gradient approximation, and the LDA+U approximation. The Jahn-Teller distortion is reproduced even by LDA but the magnitude of the distortion for all three approximations is not quite large enough compared with the experimental value. The same analysis is performed also for the hypothetical ferromagnetic state. The Jahn-Teller distortion still exists but the magnitude is much reduced. The unit-cell shape becomes nearly cubic. These features are qualitatively consistent with the related experimental observations. If the crystal structure is optimized for each magnetic state, the present band calculation predicts the ferromagnetic state to be lower in energy than the *A*-type antiferromagnetic state, which is inconsistent with the experimental observation. The origin of the failure in the prediction of the ground state is discussed. [S0163-1829(97)05142-4]

I. INTRODUCTION

Perovskite transition-metal oxides (TMO) have a long history of research and have been known as materials with a variety of interesting properties, such as dielectric, magnetic, optical, and transport properties. Renewal of interest in the perovskite TMO was brought in by the discovery of the high-T_c superconductors about a decade ago[1] and the mechanism of superconductivity and the basic properties of the strongly correlated systems have been discussed intensively.

In addition to the high-T_c related activities, we have also found recently very important activities for the perovskite manganites. Colossal magnetoresistance,[2–6] magnetic-field-(H-) induced structural phase transition[7] and very unique phase diagrams in the T-H plane,[8] are some examples of new dramatic discoveries. It is true that many of the basic ingredients in the mechanisms responsible to these phenomena were proposed in the past, such as double exchange,[9–11] Jahn-Teller (JT) effect,[12–14] charge ordering,[15,16] orbital ordering[17–19], and so on. Nevertheless, coherent understanding of various phenomena requires detailed analysis of the real controlling mechanism for each phenomenon, because some different mechanisms can lead to the same phenomena.

In the present work, we focus our attention on the relation between the JT effect and the magnetic structure in $LaMnO_3$, which is the mother material of many manganites exhibiting interesting phenomena. The importance of the JT effect and its relation to magnetic properties have already been discussed by several authors. Millis *et al.* claimed that not only the double exchange mechanism but also the dynamical JT effect will contribute to colossal magnetoresistance.[20] The observed temperature dependence of the Debye-Waller factor for oxygen of $La_{0.65}Ca_{0.35}MnO_3$ follows qualitatively the behavior as predicted by their theory.[21] There are also observations that the temperature dependence of the Mn-O bond below and above T_c is different.[22,23] In the mother material $LaMnO_3$, it was demonstrated that the ground-state *A*-type antiferromagnetic (AF) order is stabilized only by taking the JT distortion into account.[24,25] The JT distortion induces the orbital polarization (and ordering) in which the orbitals confined in the ab plane, $d_{3x^2-r^2}$ or $d_{3y^2-r^2}$, are dominantly populated and the counter orbitals of e_g symmetry, $d_{z^2-y^2}$ or $d_{z^2-x^2}$, are less populated. This orbital ordering reduces the ferromagnetic (FM) contribution from the e_g orbitals to the interlayer exchange coupling making the AF contribution from the t_{2g} orbitals dominant.

There is a one-to-one correspondence between the JT distortion and the orbital polarization. As the e_g (or t_{2g}) band is the antibonding state between the oxygen p orbital and the transition-metal d orbital, the e_g (or t_{2g}) state with the d orbital extending along the longer Mn-O bond has a lower energy and thus will be more populated than the opposite case. However, it is not obvious which one of the two, the JT distortion or the orbital polarization, is the trigger for the other. It is well known that the orbital polarization can be induced also by the electron-electron interaction. For example, in the Hartree-Fock approximation for an impurity problem with orbital degeneracy, the instability condition for the orbital polarization is given by

$$U_{\mathrm{eff}} D(E_f) \geqslant 1, \tag{1}$$

$$U_{\mathrm{eff}} = U - J, \tag{2}$$

where U (J) is the Coulomb (exchange) part of the electron-electron interaction and $D(E_f)$ is the density of states per spin per orbital at the Fermi level. If the orbital polarization is stabilized by the electron-electron interaction, the lattice will deform accordingly. In such a case the lattice distortion (we call this also JT distortion) is a result of the orbital polarization. On the other hand, in the standard JT distortion, the electron-phonon interaction in the state with orbital degeneracy will produce the lattice distortion and the orbital polarization simultaneously. It is almost impossible to judge unambiguously which of the two, the electron-electron interaction or the electron-phonon interaction, is the controlling factor in the real material. Nevertheless, we expect some qualitative differences among different materials. First, let us consider the difference between $LaVO_3$ and $LaMnO_3$. The former has the d-electron configuration of $(t_{2g})^2$ and the Fermi level sits in the t_{2g} manifold. As the t_{2g}–O $2p$ hybridization is weak, the t_{2g} states are fairly localized. Therefore we expect that the orbital polarization in $LaVO_3$ is induced mainly by the electron-electron interaction and that the lattice distortion follows the orbital polarization. On the other hand, the Fermi level of $LaMnO_3$ is in the e_g manifold with the electron configuration of $(t_{2g})^3(e_g)^1$. The strong e_g–O $2p$ hybridization makes the e_g states itinerant and we expect a strong electron-phonon interaction will cause the JT effect. Such a natural expectation for the difference between $LaVO_3$ and $LaMnO_3$ is supported by the fact that the difference between the longest V-O bond and the shortest one is only 0.06 Å in $LaVO_3$, which is much smaller than the corresponding value of 0.27 Å in $LaMnO_3$.[26]

Second, we consider the difference between $KCuF_3$ and $LaMnO_3$. In both systems, the Fermi level sits in the e_g manifold. However, as the Cu d orbital is more localized than the Mn d orbital, the lattice distortion and the orbital polarization (and ordering) can be stabilized only by taking account of $U_{\rm eff}$ explicitly with the so-called LDA+U method.[27] This suggests that the electron-phonon interaction is of secondary importance in $KCuF_3$.

The purpose of the present work is now clear. The first objective is to see how the JT distortion of $LaMnO_3$ is produced by some different levels of approximations to the electron-electron interaction. We try three approximations, the local density approximation (LDA), the generalized gradient approximation (GGA), and the LDA+U method. (We assume the spin polarization is included in all the three approximations.) The second objective is to see how the JT distortion is affected by the magnetic ordering. This is an inverse problem of our previous work where we considered the magnetic interaction as a function of the JT distortion.[24] We have found that the JT distortion of $LaMnO_3$ is stabilized even with LDA being in contrast to the case of $KCuF_3$.[27] This may imply that the electron-phonon interaction is the main origin of the JT distortion in $LaMnO_3$. However, we also have found that even the LDA+U method cannot reproduce the full magnitude of the observed JT distortion. With regard to the second objective, the JT distortion is substantially reduced and even the lattice becomes almost cubic in the FM ordering. The result is qualitatively consistent with some experimental facts.

II. CALCULATIONAL METHOD

We adopt Vanderbilt's ultrasoft pseudopotential (PP) method[28,29] and use the plane waves as a basis set in order to optimize the structure of $LaMnO_3$ efficiently. The p and f states of La, d states of Mn, and p states of O are treated by the ultrasoft PP and the other states are treated by the norm-conserving PP optimized by Troullier and Martins' prescription.[30] The cutoff energy is 30.25 Ry, which is sufficient to make the calculated lattice constant converge within 1%. The number of **k** points is 144 in the first Brillouin zone, which corresponds to 48 and 56 **k** points in the irreducible Brillouin zone for the FM and AF orderings, respectively. The linear tetrahedron method is employed to sum up the occupied states. It was confirmed that the PP method and the full-potential linear augmented plane wave (FLAPW) method give almost identical results.

The expressions proposed by Perdew *et al.*[31,32] are used for the LDA and GGA functional. In addition to LDA and GGA, we adopt the LDA+U method[33,34] as an attempt to go beyond GGA to treat strongly correlated electron systems. In the LDA+U method the space of the electronic states is separated into the subspace of the localized orbitals, for which the Coulomb interaction between electrons is explicitly taken into account, and the subspace of the delocalized states, for which the orbital independent Kohn-Sham one electron potential is considered to be a good approximation. The interaction energy between the localized electrons is assumed to be given by the Hubbard-like expression[35]

$$E^U[\{n_m^\sigma\}]=U\sum_{mm'} n_m^\uparrow n_{m'}^\downarrow+\frac{U-J}{2}\sum_{m\neq m'}(n_m^\uparrow n_{m'}^\uparrow+n_m^\downarrow n_{m'}^\downarrow), \tag{3}$$

where $\{n_m^\sigma\}$ is the set of orbital occupancies for the localized states, m and σ denote the orbital and spin, respectively, $n^\sigma=\Sigma_m n_m^\sigma$, and $n=\Sigma_\sigma n^\sigma$. The interaction between localized electrons is already included in the local-spin-density approximation (LSDA) and this part has to be subtracted to avoid double counting. In the present work, we follow the prescription given by Solovyev *et al.*:[34]

$$E^{dc}[n^\sigma]\equiv\frac{U}{2}n(n-1)-\frac{J}{2}\{n^\uparrow(n^\uparrow-1)+n^\downarrow(n^\downarrow-1)\}. \tag{4}$$

The total energy of the LDA+U method is given by

$$\begin{aligned}E^{\rm LDA+U}[\rho^{\uparrow,\downarrow},\{n_m^{\uparrow,\downarrow}\}]&=E^{\rm LSDA}[\rho^{\uparrow,\downarrow}]+E^U[\{n_m^{\uparrow,\downarrow}\}]\\&\quad-E^{dc}[n^{\uparrow,\downarrow}]\\&=E^{\rm LSDA}[\rho^{\uparrow,\downarrow}]\\&\quad+\frac{U-J}{2}\left\{n-\sum_{m,\sigma}n_m^\sigma n_m^\sigma\right\},\end{aligned} \tag{5}$$

with $E^{\rm LSDA}$ the total energy in the LSDA. We implemented this method into the PP method. Some details of the actual implementation are described in the Appendix. Note that U and J are simply parameters and $U_{\rm eff}=U-J$ is set to be 2.0 eV. This value of $U_{\rm eff}$ that is applied to both t_{2g} and e_g electrons gives a reasonable band gap for $LaMnO_3$.[36]

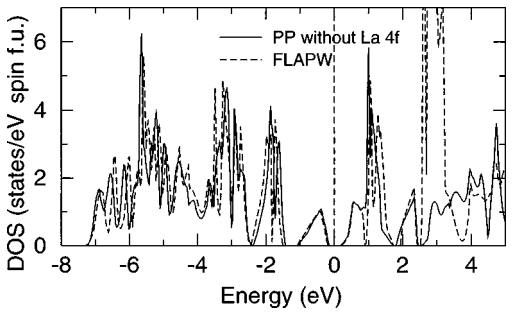

FIG. 1. Total DOS for $LaMnO_3$ obtained by the PP without the La $4f$ states (solid lines) and that obtained by FLAPW (dashed lines).

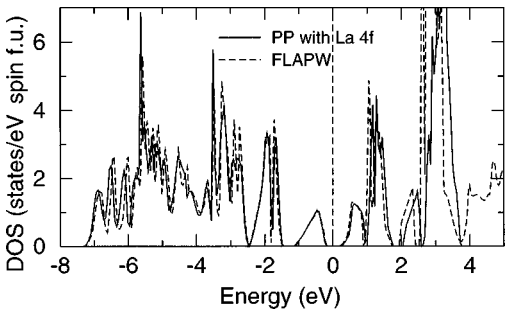

FIG. 2. Total DOS for $LaMnO_3$ obtained by the PP including the La $4f$ states (solid lines) and that obtained by FLAPW (dashed lines).

III. RESULTS AND DISCUSSION

A. Role of La $4f$ state

Because the La $4f$ states are located above the Fermi level by about 3 eV in the calculated result by FLAPW,[26] we neglected $4f$ states in the construction of a PP of La as a first attempt. The occupied part of the calculated density of states (DOS) by using the PP without La $4f$ states seems to be in reasonably good agreement with that by FLAPW as shown in Fig. 1. Thus we tried to optimize the internal coordinates of $LaMnO_3$ with this PP for the lattice constants determined experimentally. As the Jahn-Teller distortion was reduced rapidly in the optimization process, we stopped the optimization just before the system changed from an AF insulator to a FM metal. The total energy for this final structure is 480 meV/f.u. lower than that for the experimental structure. However, FLAPW gave an opposite result; i.e., the experimental structure is stabler by 198 meV/f.u. than the structure mentioned above. We also calculated the total energies of these structures by fixing the energy parameters of La $4f$ states to be about 18 eV above the Fermi level in the FLAPW calculation. This calculation reproduced the PP calculation, indicating the necessity of the La $4f$ states in the structure optimization. We can also see in Fig. 2 that inclusion of the La $4f$ states in the PP gives a DOS in better agreement with that by FLAPW compared with the former PP result: significant improvements are seen for the O $2p$ states between -4 eV and -3 eV, and for the Mn t_{2g} states located around -2 eV. The orbitals for these states extend to the La atoms.

Therefore, if we remove the La $4f$ states artificially, the contribution to the cohesion from the $2p$(O)–$4f$(La) and t_{2g}(Mn)–$4f$(La) hybridization will also be removed. This may cause positive internal pressure to the system and re-

TABLE I. The optimized structure parameters of $LaMnO_3$ for the A-type AF and for the hypothetical FM orderings. In the upper half, the results with experimental lattice constants are shown and in the lower half, those with full structure optimization are shown. The percentage shown in the parentheses denotes the difference between the optimized lattice constants and the experimental ones.

		Mn-O (a.u.)		∠Mn-O-Mn (°)		Q_2	Q_3	Lattice constants (a.u.)			Volume
		ab plane	c axis	ab plane	c axis	(a.u.)		a	b	$c/\sqrt{2}$	(a.u.^{3})
Experiment		3.597, 4.128	3.698	154	157	+0.14	0.78	10.454	10.851	10.247	1643.692
					Experimental cell						
AF	LDA	3.715, 3.967	3.696	157	157	−0.03	0.43				
	GGA	3.713, 3.977	3.698	157	157	−0.02	0.44				
	LDA+U	3.693, 3.988	3.697	158	157	+0.01	0.48				
FM	LDA	3.787, 3.885	3.695	158	157	−0.13	0.23				
	GGA	3.787, 3.890	3.696	158	157	−0.13	0.24				
	LDA+U	3.784, 3.887	3.695	158	157	−0.13	0.24				
					Optimized cell						
AF	LDA	3.702, 3.877	3.682	158	158	−0.03	0.30	10.404	10.654	10.214	1601.145
								(−0.3%)	(−1.8%)	(−0.3%)	(−2.6%)
	GGA	3.717, 4.087	3.755	156	156	+0.05	0.57	10.603	10.967	10.384	1707.617
								(+1.4%)	(+1.1%)	(+1.3%)	(+3.9%)
FM	LDA	3.731, 3.800	3.728	157	157	−0.00	0.12	10.388	10.500	10.337	1594.552
								(−0.6%)	(−3.2%)	(+0.9%)	(−3.0%)
	GGA	3.810, 3.893	3.775	158	157	−0.05	0.16	10.585	10.785	10.501	1695.264
								(+1.3%)	(−0.6%)	(+2.5%)	(+3.1%)

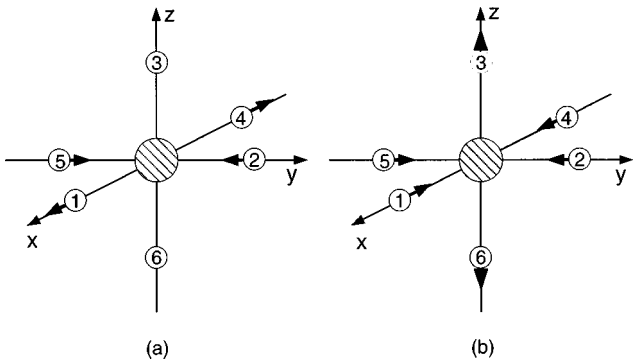

FIG. 3. (a) The normal mode Q_2 ($Q_2>0$). (b) The normal mode Q_3 ($Q_3>0$).

duce the JT distortion. We have found that the lattice constant of fcc La expands by about 4% if we remove La $4f$ states artificially.

B. Optimized structures in LDA, GGA, and LDA+U

The structure optimization of $LaMnO_3$ with AF and FM orderings was performed in two steps with LDA, GGA, and LDA+U. In the first step, we optimized only the internal coordinates fixing the lattice constants to the experimental values for the A-type AF ordering. There are 7 degrees of freedom in the internal coordinates of $LaMnO_3$. The optimized structure is characterized by the local environment around the Mn, i.e., the Mn-O bond lengths and the Mn-O-Mn bond angles in the ab plane and along the c axis, which are listed in Table I. The Jahn-Teller distortion is well specified by decomposing the lattice distortion into the normal modes Q_2 and Q_3,[12,13] which are given by

$$Q_2=\frac{1}{\sqrt{2}}(X_1-X_4-Y_2+Y_5), \tag{6}$$

$$Q_3=\frac{1}{\sqrt{6}}(2Z_3-2Z_6-X_1+X_4-Y_2+Y_5), \tag{7}$$

where X, Y, and Z are the coordinates of the surrounding oxygens with the subscript specifying the atoms as shown in Fig. 3. The oxygens that have the longest Mn-O bond are assigned to O-3 and O-6 in the present convention. For the experimental JT distortion, the tetragonal (Q_3) mode is dominant and the orthorhombic (Q_2) mode is minor and yet appreciable. The theoretical structure optimization for the A-type AF ordering with the experimental unit cell gives more than 50% (55% by LDA, 56% by GGA, and 62% by LDA+U) of the Q_3 distortion but fails to reproduce the Q_2 distortion. The underestimation of the Q_3 distortion and the incorrect estimation of the Q_2 distortion may both originate from the insufficient degree of the orbital ordering in the e_g states. In the present calculation, the occupation numbers of $d_{3x^2-r^2}$ and $d_{y^2-z^2}$ orbitals are 0.79 and 0.57, respectively in LDA, while these are 0.86 and 0.55 in LDA+U. The band structures for the optimized structures by LDA, GGA, and LDA+U are given in Fig. 4. The two band branches from -1.3 eV to the Fermi level are mainly contributed by $d_{3x^2-r^2}$ and $d_{3y^2-r^2}$ orbitals and those from the Fermi level

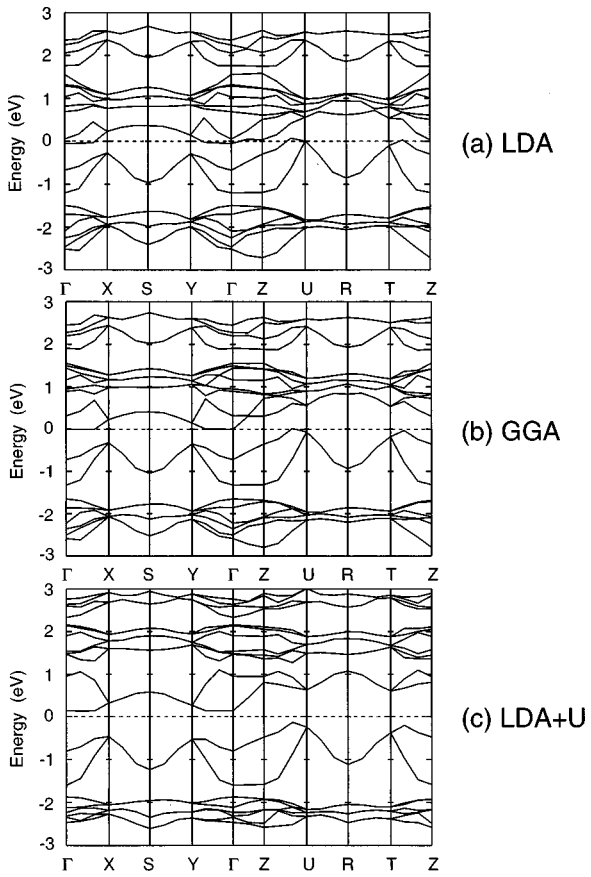

FIG. 4. Band structure for AF $LaMnO_3$ calculated in (a) LDA, (b) GGA, and (c) LDA+U. Only the internal coordinates were optimized by each approximation.

to 0.8 eV by $d_{z^2-y^2}$ and $d_{z^2-x^2}$. One can see that there is a small band overlap in both LDA and GGA and that only LDA+U can produce an insulating state for $LaMnO_3$.

If we assume a FM spin ordering keeping the unit cell the same as the experimentally obtained one for the A-type AF spin ordering, all LDA, GGA, and LDA+U give almost the same Q_2 and Q_3 as shown in Table I. Q_3 is significantly reduced and Q_2 takes a rather large negative value. However, these results are artifacts of the restriction imposed on the unit-cell shape.

In the second step of the structure optimization, we allow the unit-cell shape to relax. The unit-cell optimization was performed by calculating the stress acting on ab, bc, and ca planes. The results are summarized in Table I. (We have not optimized the unit-cell shape in LDA+U.) Let us first discuss the AF ordering case. We readily note that the Q_3 distortion is further reduced in LDA. This is mostly caused by the underestimation of the lattice constants (particularly b) in LDA. Anyway, the fact that LDA can produce an appreciable amount of the JT distortion in $LaMnO_3$ is qualitatively different from the situation in $KCuF_3$. In contrast to LDA, GGA overestimates the lattice constants as in many other cases and the estimated Q_3 distortion becomes larger though still smaller than the experimental value. The sign of Q_2 is now correct.

In Fig. 5, we plot the calculated Q_3 for three different unit-cell volumes. The result seems to suggest that the Q_3 distortion depends sensitively on the volume and that for a

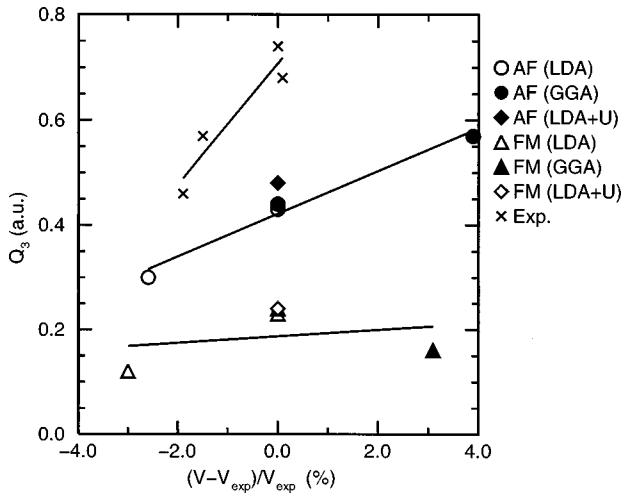

FIG. 5. The normal mode Q_3 obtained by LDA, GGA, and LDA+U are plotted as a function of the unit-cell volume. Circles and triangles correspond to the AF and FM $LaMnO_3$, respectively. Open and closed symbols are the results in LDA and GGA, respectively. Closed and open diamonds denote the Q_3 obtained in LDA+U for the AF and FM $LaMnO_3$, respectively. Experimental results for the Sr doped $LaMnO_3$ are plotted by $\times$ (Ref. 41).

given volume LDA and GGA give nearly the same Q_3. Experimentally, small doping of Sr changes the volume and Q_3 as shown in Fig. 5. In this case the slope of Q_3 against the unit-cell volume is about two times steeper than that for the calculated result. The difference in slope between theory and experiment may have two causes. First, the carrier doping will reduce the JT distortion and, second, the present calculation underestimates the JT distortion.

The full structure optimization for the FM ordering modifies the lattice constants appreciably and reduces the JT distortion. Experimentally, the doped FM state may not have any static JT distortion, while the present calculation predicts the presence of small static JT distortion in the hypothetical FM state of undoped $LaMnO_3$. We must note again that doping will efficiently destroy static cooperative JT distortion.[37] The FM state will have a wide metallic e_g band as shown in Fig. 6.

As has been discussed so far, the Jahn-Teller distortion, namely, the modulation in the Mn-O bond lengths, strongly correlates with the magnetic structure and the lattice constants. In contrast to this, the variation in the Mn-O-Mn bond angle among different situations in Table I is only about 1%. This may imply that the Mn-O-Mn bond angle is fairly in-

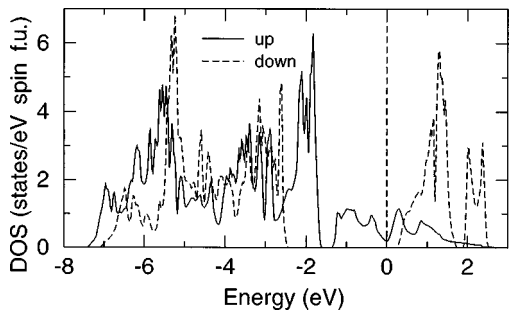

FIG. 6. Total DOS of up and down spin states for FM $LaMnO_3$ obtained in GGA for the fully optimized structure.

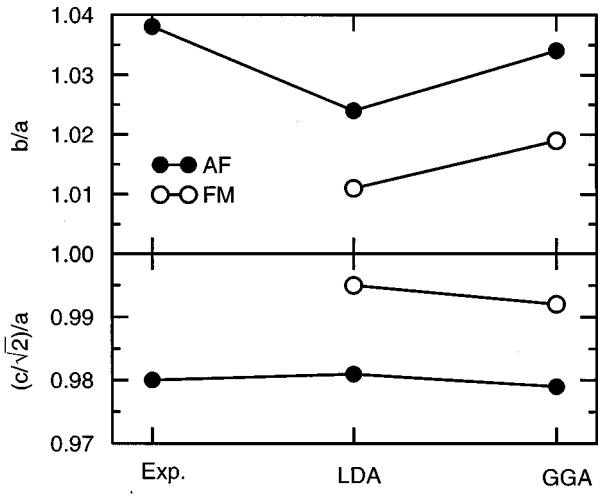

FIG. 7. The ratios of lattice constants, b/a and $(c/\sqrt{2})/a$, obtained by the experiment (Ref. 42), LDA and GGA. Closed and open circles denote the ratios for the AF and FM $LaMnO_3$, respectively.

sensitive to the external perturbations such as magnetic field, pressure, and so on. Such an observation is consistent with the argument by Hwang *et al.*:[38] by plotting the FM Curie temperature T_C, Mn-O bond lengths, and Mn-O-Mn angles as functions of the average ionic radius of the A site ions, they found that T_C correlates more strongly with the Mn-O bond length than with the Mn-O-Mn angle.

Figure 7 shows the ratios of lattice constants, b/a and $(c/\sqrt{2})/a$, for AF and FM $LaMnO_3$. For the AF $LaMnO_3$ the calculated results agree with the experiment within 2%. Clearly, the lengths of a, b, and $c/\sqrt{2}$ become closer to each other in the FM state. Experiments for $La_{1-x}Sr_xMnO_3$ indicate that b decreases, a slightly decreases, and c increases by increasing the Sr concentration x, causing the phase transition from AF to FM and from the orthorhombic to rhombohedral structure.[39] The experimental behavior is consistent with the calculated results.

Table II shows the total energy difference between the AF and FM spin orderings. Though the AF phase is stabler than the FM phase for the experimental structure, the energy ordering is reversed after the structure optimization. The failure in predicting the stable magnetic ordering for the optimized lattice structure may be due to the underestimation of the Jahn-Teller distortion and therefore the underestimation of the orbital ordering in the AF $LaMnO_3$. The A-type AF ordering in $LaMnO_3$ can be stabilized only with strong orbital ordering.[24,25] The present LDA+U gives almost the same energies for the AF and FM states even for the experimental structure, which is an even worse result than those of

TABLE II. The total energy difference (meV/f.u.) between the AF and FM $LaMnO_3$, that is $E_{AF}-E_{FM}$. ''Expt.'' and ''Opt.'' denote the experimental and optimized structures, respectively.

	Expt.	Opt.
LDA	−19.4	56.5
GGA	−15.2	62.6
LDA+U	−0.1	

LDA and GGA. The reason is that in the present LDA+U method, unlike our LDA+U_2 method,[35] the same U_{eff} is applied to both t_{2g} and e_g states. This enhances the exchange splitting in the t_{2g} states and reduces their antiferromagnetic contribution to the exchange coupling. At present we have no clear idea about the basic origin of the failure in predicting the ground state of $LaMnO_3$. Nevertheless, we comment on two possible problems in the present work. First, we speculate that the e_g bandwidth may be overestimated in the band-structure calculation and that the wider e_g band may lead to the weaker orbital polarization. The width of the e_g band is controlled by the *p-d* hybridization matrix element, the *p-d* band separation, and the electron correlation. There is no clear evidence showing that the former two factors contribute to widening the e_g band but the electron correlation, which is not properly taken into account in the present band calculation, will certainly reduce the e_g bandwidth. Second, it may be possible to improve the situation if the orbital-dependent U_{eff} is introduced in the LDA+U approach. In order to cure the inconvenient aspects of the present LDA+U approach, U_{eff} has to be very small for the t_{2g} states. Our LDA+U_2 method actually predicted that the U_{eff} for the t_{2g} states is vanishingly small for $LaMnO_3$. However, this method did not give any prescription to estimate U_{eff} for the e_g states. Developing an improved LDA+U method is one of our main goals.

Based on the arguments so far and also those in our previous work, we would like to make a comment on the appearance of the FM state by doping of divalent elements. It is generally believed that the double exchange mechanism by the doped holes is responsible for the stability of the FM state. There will be another mechanism: as was repeatedly mentioned, doping of divalent elements will certainly reduce the JT distortion, which in turn will stabilize the FM state.

IV. SUMMARY

The structure optimization for $LaMnO_3$ was performed by the plane-wave basis pseudopotential method with Vanderbilt's ultrasoft pseudopotential. The electron-electron interaction was treated by LDA, GGA, and LDA+U. The present calculation reproduces the JT distortion by about 40% to 75% depending on the approximations for the electron-electron interaction. However, this variation in the calculated JT distortion correlates with the variation in the calculated lattice constants. For given lattice constants both LDA and GGA produce nearly the same JT distortion. The present result suggests that the JT distortion decreases as the volume decreases. Anyway, even LDA can produce an appreciable JT distortion for $LaMnO_3$, in clear contrast to the situation in $KCuF_3$. We also studied the hypothetical FM state of $LaMnO_3$. The lattice becomes nearly cubic ($a \simeq b \simeq c/\sqrt{2}$) and the JT distortion is significantly suppressed.

As for the stability of the *A*-type AF spin ordering, if we fix the crystal structure as experimentally observed, the *A*-type AF state has a lower energy than the FM state. However, if we optimize the crystal structure for *A*-type AF and FM states separately, the FM state becomes stabler than the *A*-type AF state being inconsistent with the experimental fact. The failure in the prediction of the ground-state magnetic state may be due to the insufficient degree of the orbital ordering. Some possible origins of the failure were discussed.

ACKNOWLEDGMENTS

The present work is partly supported by New Energy and Industrial Technology Development Organization (NEDO) and also by the Grant-in-Aid for Scientific Research from the Ministry of Education, Science and Culture of Japan.

APPENDIX: IMPLEMENTATION OF THE LDA+U METHOD IN THE PSEUDOPOTENTIAL METHOD

The LDA+U method has been so far implemented in the electronic structure calculations using the atomic orbital-like basis: the linearized muffin-tin orbital (LMTO) method[33] and the linear combination of atomic orbitals (LCAO).[40] In the present work we implemented the LDA+U method in the pseudopotential method with Vanderbilt's ultrasoft pseudopotential. For that purpose the first-order density matrix γ^{σ}_{mn} is defined as follows:

$$\gamma^{\sigma}_{m} \equiv \sum_{k,i} f^{\sigma}_{k,i} \langle \chi^{\sigma}_{m} | \psi^{\sigma}_{k,i} \rangle \langle \psi^{\sigma}_{k,i} | \chi^{\sigma}_{n} \rangle \tag{A1}$$

$$= \sum_{k,i} f^{\sigma}_{k,i} \langle \tilde{\chi}^{\sigma}_{m} | \hat{S} | \tilde{\psi}^{\sigma}_{k,i} \rangle \langle \tilde{\psi}^{\sigma}_{k,i} | \hat{S} | \tilde{\chi}^{\sigma}_{n} \rangle, \tag{A2}$$

where $\psi^{\sigma}_{k,i}$ and $\tilde{\psi}^{\sigma}_{k,i}$ are true and pseudo wave functions, respectively, and $\hat{S}$ is a Hermitian overlap operator.[28,29] χ^{σ}_{m} and $\tilde{\chi}^{\sigma}_{m}$ are true and pseudo atomic orbitals, respectively. The diagonalized density matrix $\tilde{\gamma}^{\sigma}_{mn}$ is written as

$$\tilde{\gamma}^{\sigma}_{mn} = \sum_{k,i} f^{\sigma}_{k,i} U^{\sigma *}_{m'm} \langle \tilde{\chi}^{\sigma}_{m'} | \hat{S} | \tilde{\psi}^{\sigma}_{k,i} \rangle \langle \tilde{\psi}^{\sigma}_{k,i} | \hat{S} | \tilde{\chi}^{\sigma}_{n'} \rangle U^{\sigma}_{n'n} = \delta_{mn} n^{\sigma}_{m}, \tag{A3}$$

where $U^{\sigma}_{n'n}$ is a unitary matrix diagonalizing the density matrix, and n^{σ}_{m} are eigenvalues. The total energy of the LDA+U method is calculated by Eq. (5) with n^{σ}_{m} of Eq. (A3). The Kohn-Sham equation in LDA+U is given by

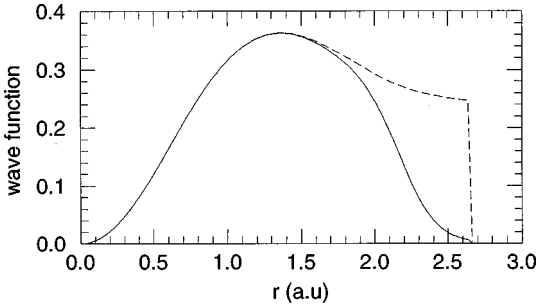

FIG. 8. The dashed line is the pseudo wave function obtained in the procedure of producing the pseudopotential of Mn. It vanishes beyond the muffin-tin radius of 2.64 a.u., because the calculated result by LMTO is used for making the pseudopotential. The solid line is the truncated pseudo wave function by using $r_c = 2.2$ a.u. and $d = 0.12$ a.u.

$$(\hat{\mathcal{H}}^{\mathrm{LDA+U}}-\varepsilon^{\sigma}_{k,i}\hat{S})|\tilde{\psi}^{\sigma}_{k,i}\rangle$$
$$=(\hat{\mathcal{H}}^{\mathrm{LSDA}}-\varepsilon^{\sigma}_{k,i}\hat{S})|\tilde{\psi}^{\sigma}_{k,i}\rangle+(U-J)\sum_{m}\left(\frac{1}{2}-n^{\sigma}_{m}\right)\frac{\delta n^{\sigma}_{m}}{\delta f^{\sigma}_{k,i}\tilde{\psi}^{\sigma*}_{k,i}}$$
$$=0, \tag{A4}$$

with

$$\frac{\delta n^{\sigma}_{m}}{\delta f^{\sigma}_{k,i}\tilde{\psi}^{\sigma*}_{k,i}}=\hat{S}|\tilde{\chi}^{\sigma}_{n'}\rangle U^{\sigma}_{n'm}U^{\sigma*}_{m'm}\langle\tilde{\chi}^{\sigma}_{m'}|\hat{S}|\tilde{\psi}^{\sigma}_{k,i}\rangle$$
$$=\left\{|\tilde{\chi}^{\sigma}_{n'}\rangle+\sum_{n''m'',I}q^{I}_{n''m''}|\beta^{I}_{n''}\rangle\langle\beta^{I}_{m''}|\tilde{\chi}^{\sigma}_{n'}\rangle\right\}$$
$$\times U^{\sigma}_{n'm}U^{\sigma*}_{m'm}\left\{\langle\tilde{\chi}^{\sigma}_{m'}|\tilde{\psi}^{\sigma}_{k,i}\rangle\right.$$
$$\left.+\sum_{n'''m''',I}q^{I}_{n'''m'''}\langle\tilde{\chi}^{\sigma}_{m'}|\beta^{I}_{n'''}\rangle\langle\beta^{I}_{m'''}|\tilde{\psi}^{\sigma}_{k,i}\rangle\right\}. \tag{A5}$$

As for the definition of the quantities in Eq. (A5), see Refs. 28 and 29.

There is an ambiguity in the choice of the atomic orbital in Eq. (A2). A truncated pseudo wave function is chosen as the pseudo atomic orbital, which is defined by the following expression:

$$\tilde{\chi}^{\sigma}_{m}=\tilde{\varphi}_{m}/[1+\exp\{(r-r_{c})/d\}], \tag{A6}$$

where $\tilde{\varphi}_{m}$ is the pseudo wave function obtained in the procedure of producing the pseudopotential, r_c and d are the cutoff radius and width of the truncation. Figure 8 shows the truncation of the pseudo wave function for Mn. The pseudo atomic orbitals are then normalized so as to satisfy $\langle\tilde{\chi}^{\sigma}_{m}|\hat{S}|\tilde{\chi}^{\sigma}_{m}\rangle=1$.

[1] J. G. Bednorz and K. A. Muller, Z. Phys. B **64**, 189 (1986).
[2] R. M. Kusters, J. Singleton, D. A. Keen, R. McGreevy, and W. Hayes, Physica B **155**, 362 (1989).
[3] K. Chahara, T. Ohno, M. Kasai, and Y. Kozono, Appl. Phys. Lett. **63**, 1990 (1993).
[4] R. von Helmolt, J. Wecker, B. Holzapfel, L. Schultz, and K. Samwer, Phys. Rev. Lett. **71**, 2331 (1993).
[5] S. Jin, T. H. Tiefel, M. McCormack, R. A. Fastnacht, R. Ramesh, and L. Chen, Science **264**, 413 (1994).
[6] Y. Tokura, A. Urushibara, Y. Moritomo, T. Arima, A. Asamitsu, G. Kido, and N. Furukawa, J. Phys. Soc. Jpn. **63**, 3931 (1994).
[7] A. Asamitsu, Y. Moritomo, Y. Tomioka, T. Arima, and Y. Tokura, Nature (London) **373**, 407 (1995).
[8] Y. Tokura, Y. Tomioka, H. Kuwahara, A. Asamitsu, Y. Moritomo, and M. Kasai, J. Appl. Phys. **79**, 5288 (1996).
[9] C. Zener, Phys. Rev. **82**, 403 (1951).
[10] P. W. Anderson and H. Hasegawa, Phys. Rev. **100**, 675 (1955).
[11] P.-G. de Gennes, Phys. Rev. **118**, 141 (1960).
[12] J. H. V. Vleck, J. Chem. Phys. **7**, 72 (1939).
[13] J. Kanamori, J. Appl. Phys. Suppl. **31**, 14S (1960).
[14] K. I. Kugel and D. I. Khomskii, Usp. Fiz. Nauk **136**, 621 (1982) [Sov. Phys. Usp. **25**, 231 (1982)].
[15] E. O. Wollan and W. C. Koehler, Phys. Rev. **100**, 545 (1955).
[16] J. B. Goodenough, Phys. Rev. **100**, 564 (1955).
[17] M. Cyrot and C. Lyon-Caen, J. Phys. (France) **36**, 253 (1975).
[18] Y. Ito and J. Akimitsu, J. Phys. Soc. Jpn. **40**, 1333 (1976).
[19] J. Akimitsu and Y. Ito, J. Phys. Soc. Jpn. **40**, 1621 (1976).
[20] A. J. Millis, B. I. Shraiman, and R. Mueller, Phys. Rev. Lett. **77**, 175 (1996).
[21] P. Dai, J. Zhang, H. A. Mook, S.-H. Liou, P. A. Dowben, and E. W. Plummer, Phys. Rev. B **54**, R3694 (1996).
[22] D. N. Argyriou, J. F. Mitchell, C. D. Potter, D. G. Hinks, J. D. Jorgensen, and S. D. Bader, Phys. Rev. Lett. **76**, 3826 (1996).
[23] T. A. Tyson, J. Mustre de Leon, S. D. Conradson, A. R. Bishop, J. J. Neumeier, H. Röder, and J. Zang, Phys. Rev. B **53**, 13 985 (1996).
[24] I. Solovyev, N. Hamada, and K. Terakura, Phys. Rev. Lett. **76**, 4825 (1996).
[25] T. Mizokawa and A. Fujimori, Phys. Rev. B **54**, 5368 (1996).
[26] N. Hamada, H. Sawada, and K. Terakura, in *Spectroscopy of Mott Insulators and Correlated Metals*, edited by A. Fujimori and Y. Tokura (Springer-Verlag, Berlin, 1995), p. 95.
[27] A. I. Liechtenstein, V. I. Anisimov, and J. Zaanen, Phys. Rev. B **52**, R5467 (1995).
[28] D. Vanderbilt, Phys. Rev. B **41**, 7892 (1990).
[29] K. Laasonen, A. Pasquarello, R. Car, C. Lee, and D. Vanderbilt, Phys. Rev. B **47**, 10 142 (1993).
[30] N. Troullier and J. L. Martins, Phys. Rev. B **43**, 1993 (1991).
[31] J. P. Perdew, J. A. Chevary, S. H. Vosko, K. A. Jackson, M. R. Pederson, D. J. Singh, and C. Fiolhais, Phys. Rev. B **46**, 6671 (1992).
[32] J. P. Perdew and Y. Wang, Phys. Rev. B **45**, 13 244 (1992).
[33] V. I. Anisimov, J. Zaanen, and O. K. Andersen, Phys. Rev. B **44**, 943 (1991).
[34] I. V. Solovyev, P. H. Dederichs, and V. I. Anisimov, Phys. Rev. B **50**, 16 861 (1994).
[35] I. Solovyev, N. Hamada, and K. Terakura, Phys. Rev. B **53**, 7158 (1996).
[36] N. Hamada (unpublished).
[37] A. J. Millis, Phys. Rev. B **53**, 8434 (1996).
[38] H. Y. Hwang, S.-W. Cheong, P. G. Radaelli, M. Marezio, and B. Batlogg, Phys. Rev. Lett. **75**, 914 (1995).
[39] A. Urushibara, Y. Moritomo, T. Arima, A. Asamitsu, G. Kido, and Y. Tokura, Phys. Rev. B **51**, 14 103 (1995).
[40] W. E. Pickett, S. E. Erwin, and E. C. Ethridge (unpublished).
[41] H. Kawano, R. Kajimoto, M. Kubota, and H. Yoshizawa, Phys. Rev. B **53**, R14 709 (1996).
[42] J. B. A. A. Elemans, B. V. Laar, K. R. V. D. Veen, and B. O. Loopstra, J. Solid State Chem. **3**, 238 (1971).